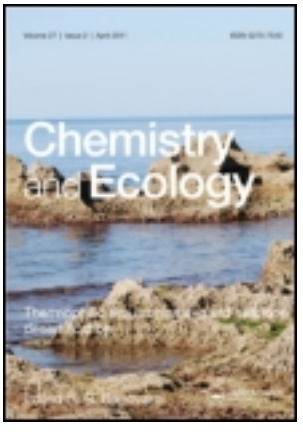

Chemistry and Ecology
Publication details, including instructions for authors and subscription information:
http://www.tandfonline.com/loi/gche20

Adsorption of phosphate ions from water using a novel cellulose-based adsorbent

Thayyath S. Anirudhan [a] & Priya Senan [a]

[a] Department of Chemistry, University of Kerala, Kariavattom, Trivandrum, 695 581, India

Available online: 04 Apr 2011

To cite this article: Thayyath S. Anirudhan & Priya Senan (2011): Adsorption of phosphate ions from water using a novel cellulose-based adsorbent, Chemistry and Ecology, 27:2, 147-164

To link to this article: http://dx.doi.org/10.1080/02757540.2010.547487

Chemistry and Ecology
Vol. 27, No. 2, April 2011, 147–164

Taylor & Francis
Taylor & Francis Group

Adsorption of phosphate ions from water using a novel cellulose-based adsorbent

Thayyath S. Anirudhan* and Priya Senan

Department of Chemistry, University of Kerala, Kariavattom, Trivandrum-695 581, India

(*Received 11 May 2010; final version received 19 October 2010*)

A novel cellulose-based adsorbent, iron(III)-coordinated amino-functionalised poly(glycidylmethacrylate)-grafted cellulose [Fe(III)–AM-PGMACell] was developed for the removal of phosphate from water and wastewater. The scanning electron micrograph showed that AM-PGMACell has a rougher surface than cellulose and the adsorption of Fe(III) on AM-PGMACell made the surface even rougher. Infrared spectroscopy revealed that amino groups on the surface of AM-PGMACell complexed with Fe(III) played an important role in the removal of phosphate from solutions. X-Ray diffraction patterns showed a decrease in crystallinity after graft copolymerisation onto cellulose. The effects of contact time, initial sorbate concentration, pH, agitation speed, dose of adsorbent and temperature on the removal process were investigated. Maximum removal of 99.1% was observed for an initial concentration of $25\,mg \cdot L^{-1}$ at pH 6.0 and an adsorbent dose of $2.0\,g \cdot L^{-1}$. A two-step pseudo-first-order kinetic model and Sips isotherm model represented the measured data very well. Complete removal of $11.6\,mg \cdot L^{-1}$ phosphate from fertiliser industry wastewater was achieved by $1.6\,g \cdot L^{-1}$ Fe(III)–AM-PGMACell. The adsorbent exhibited very high reusability for several cycles. Overall, the study demonstrated that Fe(III)–AM-PGMACell can be used as an efficient adsorbent for the removal and recovery of phosphate from water and wastewater.

Keywords: cellulose; glycidyl methacrylate; graft copolymerisation; phosphate; adsorption kinetics; thermodynamic parameters

1. Introduction

The removal of phosphate from domestic, municipal and industrial effluents, particularly fertiliser industrial effluents, is an important measure to prevent eutrophication in receiving water bodies like ponds, lakes and inland seas. However, because these natural resources (phosphate ores) are rapidly being exhausted, it is necessary to develop a phosphate-recovery system from effluents. Phosphate is often present in wastewater in low concentrations, mostly as phosphates including organic phosphate, inorganic ortho phosphates, oligophosphates and polyphosphates (particulate P) [1]. The principal phosphorus compounds in wastewater are generally orthophosphates [2]. In aqueous solutions, inorganic phosphate (orthophosphates) exists as four species, H_3PO_4, $H_2PO_4^-$, HPO_4^{2-} and PO_4^{3-} at different ratios depending on pH and ionic strength [3]. Many physical and chemical methods have been employed to remove phosphate from effluents. Among the various methods cited in the literature, adsorption is comparatively more useful and

*Corresponding author. Email: tsani@rediffmail.com

ISSN 0275-7540 print/ISSN 1029-0370 online

DOI: 10.1080/02757540.2010.547487
http://www.informaworld.com

economical for the removal of phosphate from wastewaters and can be probably used for collecting and recycling of phosphate [4]. Many types of adsorbents for removing phosphate have been developed [5]. Cellulose is gaining interest in application as an adsorbent in wastewater treatment due to its biodegradable and non-toxic nature. The adsorption properties of cellulose can be improved by surface modification. Moreover, the poor mechanical properties and low density should be improved for water treatment operations. Cellulose derivatives obtained through the graft copolymerisation technique have been used as ion exchangers or chelate resins [6,7]. They have higher adsorption capacity and physical stability than cellulose. A new class of polymeric ion exchangers (chelating resins) has been employed for removing phosphate from aqueous solutions [8]. In recent years, investigations have led to the development of adsorbents loaded with metal ions, which can be employed for the removal of hazardous anions from wastewater. It has been reported that the Zr(IV)- or Fe(III)-loaded solid adsorbents have a high affinity for hazardous anions such as fluoride, arsenic and phosphate [9,10]. Among these, Fe(III) is mainly considered due to its strong affinity towards anions, environmental safety and low cost [11]. In this study, a novel adsorbent, iron(III)-coordinated amino-functionalised poly(glycidyl methacrylate)-grafted cellulose (Fe(III–AM-PGMACell) was prepared and characterised, and its fundamental adsorption behaviour for the removal of phosphate from water and wastewater was investigated.

2. Experimental procedures

2.1. *Description of study area and sampling procedure*

Fertiliser industry effluents were collected from a fertiliser factory located at Cochin, Kerala, India. This industry is situated on the bank of the Periyar river. The river discharges fresh water into the Cochin estuarine system (09°40′ to 10°12′ N; 76°10′ to 76°30′ E), which is connected to the Arabian Sea through a permanent opening, the barmouth at Cochin. Cochin is the major port on the south west of India. Like many other river systems, the Periyar river is also subjected to increasing human interference; the waterway receives a considerable amount of untreated effluent from various industrial units, including fertiliser, pesticide, oil refinery, electroplating, cement and chloralkali industries. The net effect of these discharges is irreparable damage to the flora and fauna of the water body; the productivity of this region has been considerably affected.

National Pollutant Discharge Elimination System general guidelines were followed for sampling and sample handling. The effluent sample was collected in a clean and sterilised plastic container of 10 L capacity at the end of the discharge pipe. The pH of the sample was measured using a portable pH meter (Model: Eutech pH 2700). Prefixation of the sample for dissolved oxygen content was performed using Winkler's A and B reagents at the collection site. Samples were kept refrigerated (4 °C) holding containers and brought immediately to the laboratory to minimise physico-chemical and biological changes. Samples were stored in the refrigerator for no more than 48 h at 4 °C in darkness. Frozen samples were allowed to defrost at room temperature (30 $\pm$ 2 °C) and physical and chemical analyses were performed using standard methods as described by the American Public Health Association.

2.2. *Preparation of adsorbent*

Cellulose used as a primary material for the preparation of Fe(III)–AM-PGMACell was procured from S.D. Fine-Chem. Ltd (Mumbai, India) and was used as received. The general procedure for preparation of the adsorbent is illustrated in Scheme 1. Cellulose (20 g) was soaked in 200 mL distilled water at room temperature. The cross-linking agent N,N'-methylenebisacrylamide

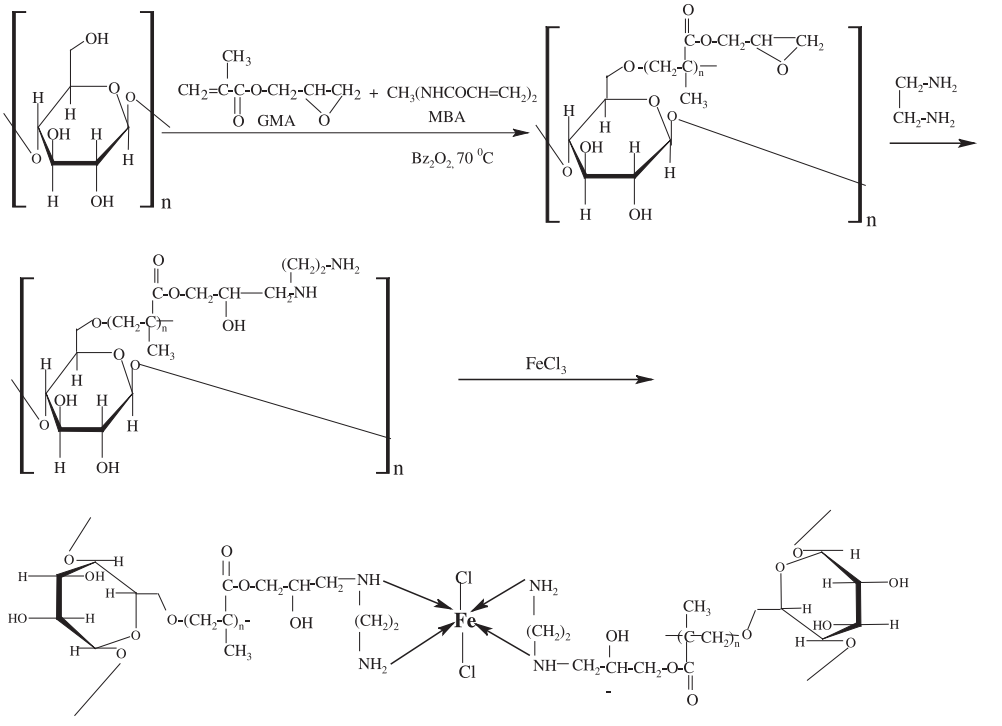

Scheme 1. Preparation of Fe(III)–AM-PGMACell.

(MBA; 0.2 g) and initiator benzoyl peroxide (Bz_2O_2; 0.2 g) were added and agitated for 5 min. The monomer glycidyl methacrylate (GMA; 19.2 mL) was added, followed by the addition of a mixture of isopropyl alcohol (2 mL) and cyclohexane (25.2 mL) in the ratio 1:12 (v/v). The contents were transferred into a flask containing 3 % poly(vinyl alcohol) (PVA; 146 mL) and reacted in a water bath at 70–80 °C with constant stirring for 3 h. When polymerisation was completed, the product was filtered, washed repeatedly with methanol to remove unreacted materials and vacuum dried at 50 °C for 6 h. Grafting yield and grafting efficiency were determined and found to be 29.8 and 112.3%, respectively. The next step was carried out by refluxing the dried mass with ethylenediamine (120 mL) and solvent 1,4-diol (200 mL), at 80 °C for 4 h. The product, amino-functionalised poly(glycidyl methracrylate)-grafted cellulose (AM-PGMACell) was separated, washed repeatedly with toluene and then distilled water, and vacuum dried at 70 °C for 5 h. The amount of amino groups in AM-PGMACell was estimated using a titration method and was found to be 1.44 mmol $\cdot$ g^{-1} [12]. Batch isotherm studies were carried out to obtain maximum loading of Iron(III) onto AM-PGMACell. Adsorption isotherms were carried out by agitating 0.1 g of AM-PGMACell with 50 mL of aqueous Fe(III) solution at eight different concentrations ranging from 50 to 400 mg $\cdot$ L^{-1} at 30 °C for 4 h and kept overnight. The adsorbent, Fe(III)–AM-PGMACell, was washed several times with distilled water, dried and passed through a set of sieves to obtain an average geometrical size of 0.096 mm and was used for phosphate removal. The amount of Fe(III) loaded was measured and was found to be 0.58 mmol $\cdot$ g^{-1}.

2.3. *Characterisation*

Fourier transform infrared (FTIR) spectra of the adsorbent samples were recorded in a Nicolet Protégé 460 spectrophotometer with the spectral region between 4000 and 450 cm^{-1} using

the KBr pellet technique. X-Ray powder diffractions were obtained with a Rigaku X-ray diffractometer using Ni-filtered Cu–K_α radiation ($\lambda = 1.541$ Å). Surface morphology was studied with a scanning electron microscope (SEM) in a Phillips XL-3CP microscope unit. The specific surface areas of the cellulose and Fe(III)–AM-PGMACell were measured by Brunauer Emmett Teller (BET), N_2 adsorption using a Quantasorb surface area analyser (QS/T). Apparent density of the adsorbent was determined using a specific gravity bottle with nitrobenzene as the displacing liquid. The anion-exchange capacity was determined by the column operation method using 0.1 M $NaNO_3$. The pH-dependent surface charge was determined by potentiometric acid–base titration as described earlier [13]. NaCl was used as background electrolyte to maintain a constant ionic strength of 0.1 M.

2.4. *Sorption studies*

A stock solution of phosphate (1000 mg · L^{-1}) was prepared by dissolving anhydrous potassium dihydrogen orthophosphate (KH_2PO_4) in distilled water and was used to prepare the adsorbate solutions by appropriate dilution.

Batch adsorption experiments were carried out in 100 mL stoppered conical flasks by mixing 0.1 g of the adsorbent with 50 mL aqueous solution of phosphate. The contents of the flasks were shaken in a temperature-controlled water bath flask shaker at 200 rpm at room temperature (30 °C). After adsorption, the phosphate concentration in the supernatant after centrifugation was determined. The amount of phosphate adsorbed was calculated from the difference between the initial and final concentrations of phosphate in equilibrium solutions. The effect of pH on the adsorption of phosphate was studied by adding 0.1 g of the adsorbent to 50 mL of phosphate solution of desired concentration (50 and 100 mg · L^{-1}). The initial pH values of the phosphate solutions were regulated to 2.0–9.0 with micro-additions of 0.1 M NaOH or 0.1 M HCl. The solutions were agitated in the water bath shaker. After equilibrium was reached, the concentration of phosphate in residual solution was determined.

Kinetic studies were carried out by adding 0.1 g of the adsorbent with 50 mL of phosphate concentrations ranging from 50 to 200 mg · L^{-1} at 30 °C in a conical flask. The initial pH of each solution was adjusted to 6.0 before mixing the adsorbent. The flasks were agitated on a shaker at 200 rpm. Samples were withdrawn at suitable intervals, centrifuged and the phosphate concentration was determined. Adsorption isotherm studies were carried out by adding 0.1 of adsorbent to a series of conical flasks filled with 50 mL of phosphate concentrations ranging from 25 to 400 mg · L^{-1}. The initial pH of the solution was adjusted to the optimum, the flasks were agitated for 2.0 h, centrifuged and the phosphate concentration in supernatant solution was analysed using the spectroscopic method [14] based on coloured complex with an acidic ammonium molybdate reagent containing ascorbic acid and potassium antimony tartarate solutions. The blue-coloured phosphate molybdate complex in solution was measured using a UV–vis spectrophotometer at 850 nm. Isotherm experiments were also conducted with 0.1 g of Dowex (Aldrich, WI, USA), a commercial chloride-form anion exchanger for comparison.

Equilibrium studies on the effect of adsorbent dose on phosphate adsorption were conducted by adding 0.02–0.20 g of the adsorbent to a series of conical flasks, each filled with 50 mL of 50.0 mg · L^{-1} of phosphate solution.

2.5. *Desorption studies*

The phosphate-loaded adsorbent was separated from the suspension in an isotherm experiment and washed with deionised water to remove any unadsorbed phosphate. The amount of phosphate adsorbed on Fe(III)–AM-PGMACell was determined. The dried spent adsorbent was mixed with

50 mL of 0.1 M NaCl solution and shaken for 2.0 h. The suspension was centrifuged, and the supernatant solution was analysed for the desorbed phosphate concentration. The adsorbent was then subjected to subsequent phosphate-loading cycles. The reusability of the adsorbent was further confirmed by repeating the adsorption–desorption cycle up to four times at 30 °C.

All the experiments were conducted in triplicate. The maximum variation with batch adsorption data among triplicate values is 4.0%. The kinetic and isotherm parameters and the model fit were demonstrated by non linear regression method using the Solver add in function on the Microsoft's Excel sheet.

3. Results and discussion

3.1. *Characterisation of the adsorbent*

Graft copolymerisation of Cell followed by amination and Fe(III) loading might create chemical modifications and therefore requires verification to support the results of the foregoing discussion. Figure 1 represents the FTIR spectra of Cell, AM-PGMACell, Fe(III)–AM-PGMACell and phosphate-loaded Fe(III)–AM-PGMACell. The broad band at 3411 cm^{-1} relative to hydrogen-bonded O–H stretching vibration and the bands at 2900 and 1028 cm^{-1} refer to the C–H stretching and C–H bending from the $–CH_2$ group and are evidenced in the IR spectrum of Cell. The pronounced signal of Cell at 1790 and 670 cm^{-1} may be relative to C=O stretching of hemicellulose and β-glycosidic linkages in Cell, respectively. The presence of amine functional groups

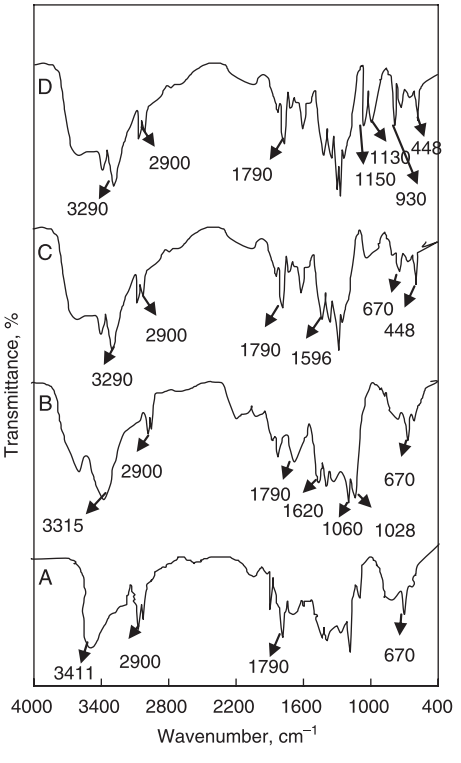

Figure 1. FTIR spectra of (a) Cell, (b) AM-PGMACell, (c) Fe(III)–AM-PGMACell and (d) phosphate-loaded Fe(III)–AM-PGMACell.

in AM-PGMACell is evidenced by the presence of new signals at 3315, 1620 and 1060 cm^{-1} relative to the N–H stretching, N–H bending and C–N stretching vibrations, which arise due to the ethylenediamine bonded to the GMA-grafted cellulose through a transamidation reaction. The N–H stretching and N–H bending frequencies were shifted to 3290 and 1596 cm^{-1}, respectively, after the adsorption of Fe(III) on the AM-PGMACell, indicating the existence of interactions between Fe(III) and the nitrogen atom in the NH_2 groups. The new peak at 448 cm^{-1} is due to Fe–N stretching vibrations. The FTIR spectrum of phosphate-loaded Fe(III)–AM-PGMACell shows three new peaks at 1130, 1152 and 930 cm^{-1} assigned to P–O stretching, P=O stretching and P–OH stretching vibrations from phosphate species, respectively [15].

X-Ray diffraction (XRD) patterns for the samples Cell, AM-PGMACell, Fe(III)–AM-PGMACell and phosphate-loaded Fe(III)–AM-PGMACell are plotted in Supplementary Figure S1 (available online only). X-ray analysis of Cell reveals that the diffraction maxima at $2\theta = 21.6$, 25.1 and 36.5° are narrow and distinct, and correspond to the crystalline domain of the cellulose structure. The scattering angles originally present in Cell at 21.6 and 36.5° are absent in AM-PGMACell, and the signal at 25.1° exhibits a considerable decrease in the intensity and sharpness of the reflection. This indicates that some rearrangement in the morphology of the cellulose chain occurs as a result of graft copolymerisation and there is also a significant decrease in crystallinity upon incorporation of the amorphous copolymer. In Fe(III)–AM-PGMACell, there is a considerable decrease in the scattering angle from 25.1 to 23.4°, which may be due to the loading of iron(III). The XRD output signal at 23.4° is wide and distinct, which may be attributed to the considerable increase in crystallinity due to the loading of Fe(III) in AM-PGMACell when compared with AM-PGMACell. From the XRD pattern after phosphate adsorption, there is a shift of the peak from 23.4 to 21.9° which suggests the presence of phosphate salt in the structure of Fe(III)–AM-PGMACell.

The scanning electron micrographs of Cell, AM-PGMACell, Fe(III)–AM-PGMACell and phosphate-loaded Fe(III)–AM-PGMACell are shown in Supplementary Figure S2 (available online only). The surface of untreated Cell was relatively smooth when compared with AM-PGMACell, Fe(III)–AM-PGMACell and phsophate–Fe(III)–AM-PGMACell. After chemical modification in Cell, the structure of AM-PGMACell became rough and is characterised by pores and cavities of different sizes. Graft copolymerisation onto Cell and introduction of the amino group through transamidation reaction on the surface of the AM-PGMACell can therefore be expected to change the material properties and thus affect Fe(III) adsorption. The micrograph of Fe(III)–AM-PGMACell reveals an irregular, loose and porous structure. The adsorption of Fe(III) on the AM-PGMACell made the surface even more rough. The SEM image obtained after the adsorption of phosphate indicates that the surface of Fe(III)–AM-PGMACell was covered with phosphate ions and the surface became smooth.

Anion-exchange capacity and apparent density values were found to be 0.71 meq $\cdot$ g^{-1} and 0.83 g $\cdot$ L^{-1} for Cell and 1.28 meq $\cdot$ g^{-1} and 1.13 g $\cdot$ L^{-1} for Fe(III)–AM-PGMACell, respectively. BET surface area of the Fe(III)-AM-PGMACell (39.9 $m^2 \cdot g^{-1}$), is higher than original Cell (18.2 $m^2 \cdot g^{-1}$). Also the total pore volume of Fe(III)–AM-PGMACell (0.37 mL $\cdot$ g^{-1}) was found to be higher than Cell (0.29 mL $\cdot$ g^{-1}). The pH_{pzc} values for Cell and Fe(III)–AM-PGMACell were found to be 5.0 and 7.5, respectively. This increase in pH_{zpc} shows that the surface of the adsorbent becomes more positive after chemical modification hence it favours the adsorption of anions below pH 7.5.

3.2. *Effect of initial pH on removal efficiency*

An understanding of the effect of pH on adsorption process is very important since the mechanism of adsorbate removal can be deduced from such a study. Bearing this in mind, the adsorption of

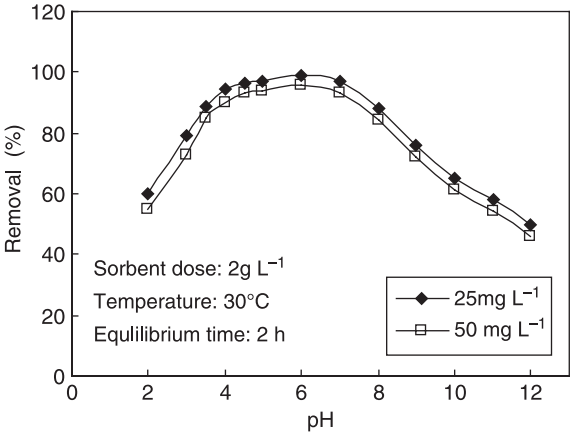

Figure 2. Effect of pH on the adsorption of phosphate onto Fe(III)–AM-PGMACell.

phosphate on Fe(III)–AM-PGMACell was studied at two different initial concentrations, 25 and 50 mg · L^{-1}, in the pH range 2.0–12.0. The results in Figure 2 show that the uptake of phosphate by the adsorbent increases with increasing pH, attaining optimum at pH 6.0, and thereafter decreased gradually. The maximum removal was 99.1 and 98.2% for phosphate concentrations of 25 and 50 mg · L^{-1}, respectively. The effect of pH can be explained in terms of pH_{pzc} of the adsorbent. The pH_{pzc} of Fe(III)–AM-PGMACell was found to be 7.5 and below this pH the surface of the adsorbent is positive, whereas above this pH the surface is negative. In addition to the neutral species, phosphate can exist in different ionic species as monovalent $H_2PO_4^-$, divalent HPO_4^{2-} and trivalent PO_4^{3-} ions, depending on the pH of the solution. ($pK1 = 2.15$, $pK2 = 7.20$ and $pK3 = 12.33$) [16]. In the pH range of 2.0–7.0, the predominant species of phosphate is $H_2PO_4^-$, whereas it is transitioned into HPO_4^{2-} at pH >7.0. Because maximum adsorption was attained at the pH 6.0 the single charged species ($H_2PO_4^-$) favours the adsorption of phosphate onto Fe(III)–AM-PGMACell. The adsorption mechanism can be considered as ion exchange occurring between Cl^- ion from the adsorbent surface and $H_2PO_4^-$ species in solution and is represented as

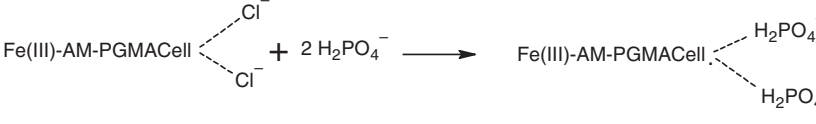

(1)

The decrease in phosphate adsorption above pH 6.0 is likely attributed to the fact that a higher pH causes Fe(III)–AM-PGMACell to carry more negative charge, thereby significantly repulsing the negatively charged species in solution. Therefore, the lower adsorption of phosphate at higher pH values resulted from increased repulsion between the more negatively charged PO_4^{3-} species and negatively charged surface sites.

3.3. *Effect of agitation speed*

The effect of agitation speed on the amount of phosphate adsorbed was studied by varying the speed of agitation from 25 to 400 rpm while maintaining the initial phosphate concentration, the dose of Fe(III)–AM-PGMACell and the initial pH of the solution constant. The results reported in Figure 3 showed that removal efficiency increased with increasing agitation rate. When the agitation speed increased from 25 to 200 rpm, the removal efficiency increased from 67.4 to

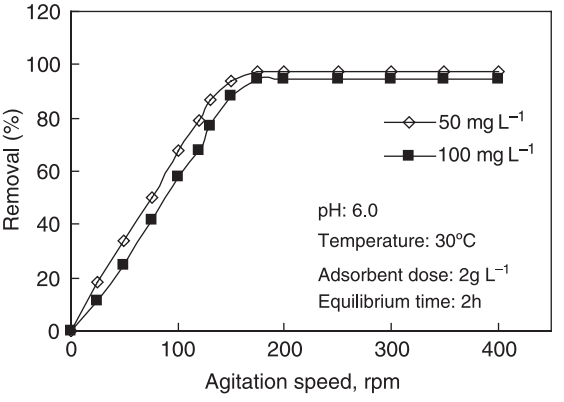

Figure 3. Effect of agitation speed on the adsorption of phosphate ions onto Fe(III)–AM-PGMACell.

97.5% for an initial concentration of 25 mg L^{-1} and 56.9 to 94.6% for 100 mg L^{-1}. The increase in the removal efficiency may be due to the fact that increasing agitation speed from 25 to 200 rpm reduced the film boundary layer surrounding the particles, thus increasing the external film transfer coefficient, and hence the adsorption capacity. A further increase in agitation speed from 200 to 400 rpm does not cause a considerable increase in the amount of phosphate adsorbed. This may be attributed to the negligence of external mass transfer for agitation speeds >200 rpm [17]. It was seen that an agitation speed of 200 rpm gives the maximum interaction of phosphate ions onto the adsorbent and hence it was selected as the optimum speed for the remaining adsorption studies.

3.4. *Effect of temperature and contact time*

The adsorption kinetics of phosphate onto Fe(III)–AM-PGMACell was investigated at various temperatures with a fixed initial concentration of 50 mg · L^{-1}. The adsorption rate was rapid during the first 30 min, thereafter it became gradual until it attained equilibrium at 2.0 h, as shown in Figure 4. Thus a shaking time of 2 h was selected for further studies. The kinetic plots indicate that with an increase in temperature from 20 to 50 °C, the percentage adsorption of phosphate decreased from 97.2% (24.3 mg · g^{-1}) to 91.3% (22.8 mg · g^{-1}), indicating that the adsorption of phosphate ions was favoured at lower temperatures. The amount of phosphate adsorbed decreased

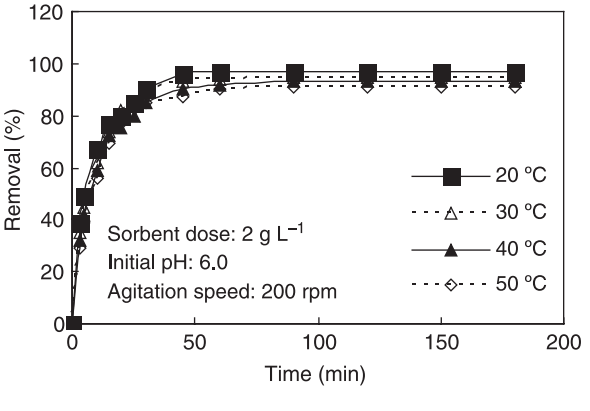

Figure 4. Effect of contact time and temperature on removal efficiency of phosphate ions by Fe(III)–AM-PGMACell.

with increasing temperature of the system and this maybe due to escaping tendency of phosphate ions from the solid phase to the bulk phase.

3.5. *Effect of initial concentration and kinetics of adsorption*

Experiments were conducted to study the effect of varying the initial phosphate concentration (25–100 mg · L^{-1}) on phosphate removal by Fe(III)–AM-PGMACell at 30 °C and the results are shown in Figure 5. The plots are single, smooth, continuous and equilibrium was attained within 2 h. It was observed that the amount adsorbed increased with increased initial phosphate concentration from 11.9 mg · g^{-1} (95.0%) to 43.6 mg · g^{-1} (87.8%) when the initial concentration increased from 25 to 100 mg · L^{-1}. The increase in uptake capacity of Fe(III)–AM-PGMACell with the increase of initial concentration is due to higher availability of phosphate ions in the solution, for the adsorption process. Another factor in the higher uptake is the increased driving force needed to overcome all mass transfer resistance of phosphate ions between the aqueous and solid phases, resulting in a higher probability of collision between the unadsorbed phosphate ions and sorbents. Similar results were reported for the adsorption of phosphate from aqueous solutions onto fly ash [18]. To investigate the mechanism of adsorption, models of two step pseudo-first-order adsorption and intraparticle diffusion were used to test adsorption kinetic data. According to the computer simulation, the two step kinetic rate equation is given as [19]:

$$q_t = q_{t,1}\left(1 - e^{-k1_1 t}\right) + q_{t,2}\left(1 - e^{-k2_1 t}\right), \tag{2}$$

where q_t is the amount of phosphate ion adsorbed at time t (mg g^{-1}), k_1 and k_2 are the kinetic rate constants in (min^{-1}) associated with first-order model at different kinetic steps, $q_{t,1}$ and $q_{t,2}$ are their pre-exponential amplitude terms. At $t = \infty$, $q_{t,1} + q_{t,2} = q_e$, the amount of phosphate ions adsorbed at equilibrium. At $t = 0$, the adsorption does not start so that $q_e = 0$. As the adsorption of phosphate ions onto Fe(III)–AM-PGMACell proceeds, the value of the exponential term in the right hand side of the Equation (2) decline initially. As adsorption proceeds, the exponential term gradually approaches zero when q_t approaches the equilibrium amount of adsorption (q_e), i.e. $q_t = 0$. The rate constants k_1 and k_2 associated with different kinetic steps can be determined using the above equation. It is also seen that in all the plots there is initial linear portion (1–30 min) which reflects the adsorption stage followed by a plateau (after 30 min) where sorption process virtually completes. Table 1 lists the results of amount adsorbed at equilibrium time (q_e) and the kinetic rate constants associated with the fast and the slow step (k_1, k_2) calculated by non-linear regression analysis using the program ORIGIN, version 7.5. The values of the correlation coefficient R^2 are

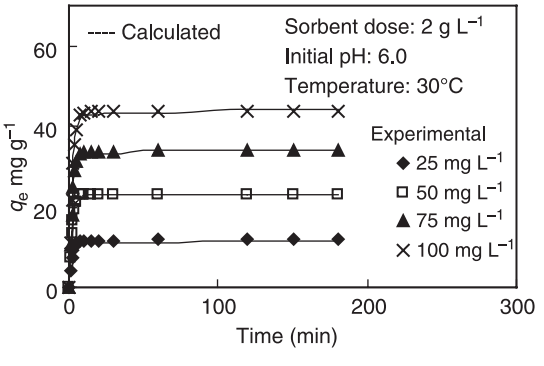

Figure 5. The effect of initial concentration on the adsorption of phosphate onto Fe(III)–AM-PGMACell and comparison of experimental and calculated adsorption kinetic data.

Table 1. Pseudo-first-order model parameters of phosphate adsorption kinetics onto Fe(III)–AM-PGMACell.

C_0 (mg · L^{-1})	q_e (mg · g^{-1})	k_1 (min^{-1})	k_2 (min^{-1})	R^2	χ^2
25	11.5	0.438	0.187	0.998	0.129
50	23.1	0.411	0.165	0.999	0.120
75	33.7	0.387	0.135	0.996	0.222
100	43.1	0.354	0.116	0.998	0.199

extremely high (>0.9960) and the adsorption capacities calculated from Equation (2) are very close to those determined experimentally, as illustrated in Figure 5. Hence it can be concluded that two step pseudo-first-order adsorption model can be used to describe the adsorption kinetics of phosphate onto Fe(III)–AM-PGMACell. The values of q_e increased but the values of k_1 and k_2 decreased with the increase in the initial phosphate concentrations. The decrease in the magnitude of k_1 and k_2 may be due to the transfer of phosphate ions from the bulk to the surface-bound phase, which would result in a more rapid uptake of the phosphate ions. It is also noted that the magnitude of k_1 is greater than k_2. This may be attributed to the initial progress of adsorption over time, as a result of which the surface of Fe(III)–AM-PGMACell become crowded with adsorbed anions. After a certain amoun of time has lapsed, the adsorbed phosphate ions tend to orient in regular fashion, thereby leading to the formation of additional vacant spaces for further adsorption from bulk to the surface [20].

Adsorption kinetics is usually controlled by different mechanisms, of which the most general is the diffusion mechanism. The anions are most probably transported from the bulk of solution into the solid phase by intraparticle diffusion, which is often the rate-limiting step in many adsorption processes. The intraparticle diffusion model is expressed with the equation given by Weber and Morris:

$$q_t = k_{\text{int}} t^{0.5} + C, \tag{3}$$

where q_t is the amount of anion adsorbed at time t, k_{int} is the intraparticle diffusion rate constant (mg · g^{-1} · min$^{1/2}$) and C is a constant representing the effect of boundary layer thickness (mg · g^{-1}). The intraparticle diffusion plots of q_t vs. $t^{0.5}$ at different phosphate concentrations are represented in Figure 6. The results showed that the plots presented a multilinearity, which indicated that two or more steps occurred in the adsorption process. From the plots, for all the concentrations studied, the first straight line representing the fast step signifies that the phosphate ions are transported to the external surface of Fe(III)–AM-PGMACell through film diffusion and

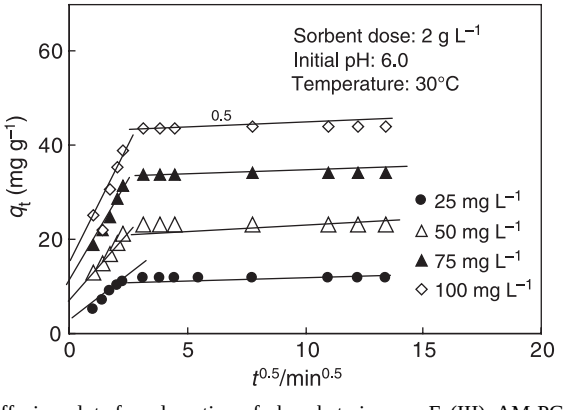

Figure 6. Intraparticle diffusion plots for adsorption of phosphate ions on Fe(III)–AM-PGMACell at different initial concentrations.

Table 2. Intraparticle kinetic parameters for phosphate adsorption onto Fe(III)–AM-PGMACell.

C_0 (mg · L^{-1})	k_{int} (mg · g^{-1} · min$^{1/2}$)	R^2	χ^2
25	1.45	0.999	0.111
50	1.76	0.998	0.122
75	2.91	0.999	0.116
100	3.88	0.997	0.133

hence its rate is fast. This is followed by the slow step, in which the intraparticle diffusion of the phosphate ions takes place through the pores of the adsorbent which is represented by the second straight line. According to this model, the q_t vs. $t^{0.5}$ plots should be linear if intraparticle diffusion is involved in the adsorption process and if these lines pass through the origin then intraparticle diffusion is the rate-controlling step. As seen from the plots, the lines does not pass through the origin, which indicates that both film diffusion and intraparticle diffusion occur simultaneously during the adsorption of phosphate on to Fe(III)–AM-PGMACell [21]. A good correlation of the data for the observed linear potion indicates that intraparticle diffusion is the rate-determining step. Intraparticle rate constant k_{int} values were obtained from the slope of the observed straight line portions of the plot of q_t vs. $t^{0.5}$ for various phosphate concentrations (Table 2). It was found that the rate constant increases with increasing phosphate concentration.

3.6. *Adsorption isotherms*

Adsorption isotherms describe how adsorbates interact with adsorbents and so are critical in optimising the use of adsorbents. Figure 7 shows adsorption isotherms, the relationship between the amount of phosphate adsorbed per unit mass of Fe(III)–AM-PGMACell (q_e; mg · g^{-1}) and its final concentration in the solution (C_e) at different temperatures. All the isotherms are positive, regular and concave to the concentration axis. Adsorption capacity increases with the increase in the concentration of phosphate ions in the aqueous phase. Figure 7 shows that Fe(III)–AM-PGMACell has a good adsorption capacity towards phosphate. A sharp increase in capacity was observed at lower initial concentration. Because the adsorption is sensitive to change under low electrolyte concentrations, electrostatic attraction (physical adsorption) plays a significant role in the complex formation between Fe(III) from the adsorbent surface and phosphate. At high concentrations, adsorption is insensitive to the change and the adsorbent displays an impressive ability to coordinate with phosphate ions. Three isotherms, namely, Langmuir [22], Freundlich [23] and Sips [24] were used to fit the experimental isotherm data

$$\text{Langmuir equation: } q_e = \frac{Q^o b_L C_e}{1 + b_L C_e}, \tag{4}$$

where Q° and b_L are Langmuir adsorption constants related to adsorption capacity and binding energy of adsorption, respectively. The equation assumes that the adsorption energy of each molecule is the same, independent of the surface of material, adsorption takes place only on some sites and there are no interactions between the molecules.

$$\text{Freundlich equation: } q_e = K_F C_e^{1/n_F}, \tag{5}$$

where K_F and $1/n_F$ are Freundlich's constants related to adsorption capacity and the heterogeneity factor, respectively. This empirical model can be applied to non-ideal adsorption on heterogeneous

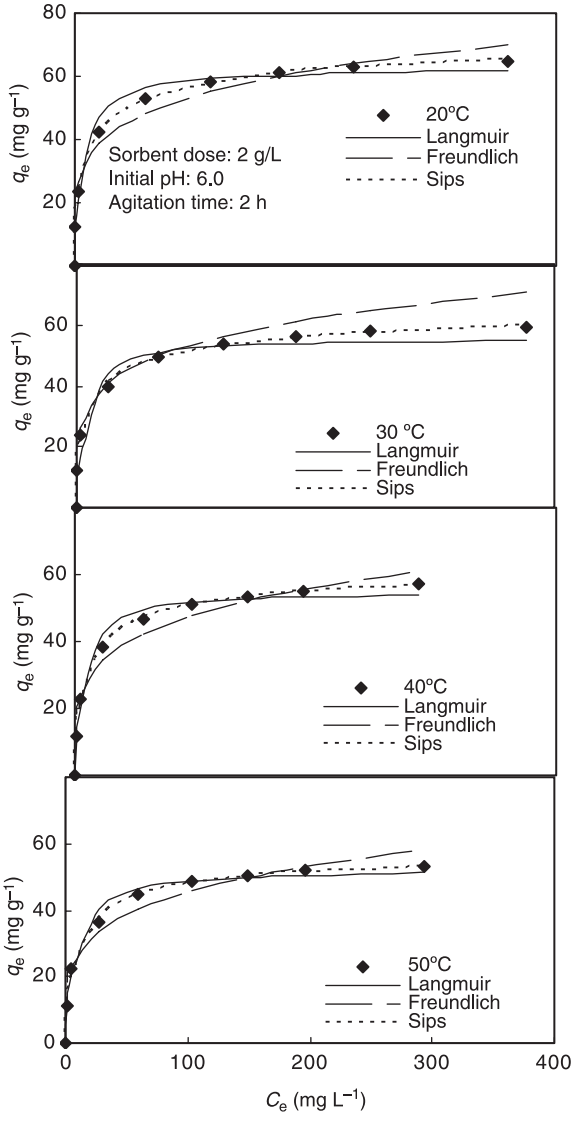

Figure 7. Effect of temperature on the adsorption of phosphate onto Fe(III)–AM-PGMACell and comparison of experimental and calculated adsorption isotherm data.

surfaces as well as multilayer adsorption.

$$\text{Sips \{Langmuir–Freundlich (L–F)\} isotherm equation: } q_e = \frac{b_s q_m C_e^{1/n_s}}{1 + b C_e^{1/n_s}} \quad (6)$$

where q_m, b_s and $1/n_s$ are Sips maximum adsorption capacity, equilibrium constant related to adsorption capacity and surface heterogeneity, respectively. At low sorbate concentrations, this equation effectively reduces to a Freundlich isotherm, whereas at high sorbate concentrations it predicts a monolayer adsorption capacity characteristic of the Langmuir isotherm. For a highly heterogeneous system, the deviation of $1/n_s$ from unity will be higher. The estimated isotherm parameters for phosphate adsorption onto Fe(III)–AM-PGMACell are summarised in Table 3.

Table 3. Isotherm parameters for the adsorption of phosphate ions onto Fe(III)–AM-PGMACell.

	Langmuir				Freundlich				Sips				
Temp (°C)	Q° (mg · g^{-1})	b_L (L · mg^{-1})	R^2	χ^2	K_F	$1/n$	R^2	χ^2	q_m (mg · g^{-1})	b_s (L · mg^{-1})	$1/n_s$	R^2	χ^2
20	62.6	0.204	0.957	1.1	22.1	0.206	0.926	9.6	77.2	0.545	0.348	0.998	0.12
30	56.1	0.182	0.966	2.5	20.6	0.212	0.922	8.7	70.1	0.116	0.515	0.997	0.15
40	55.3	0.144	0.973	3.6	17.1	0.225	0.918	6.6	58.1	0.044	0.665	0.999	0.13
50	52.7	0.121	0.987	3.1	15.8	0.230	0.925	7.5	50.3	0.017	0.725	0.998	0.12

As can be seen from Table 3, the values of R^2 and χ^2 demonstrated good agreement of the experimental data with the Sips model for the adsorption of phosphate onto Fe–AM-PGMACell. Comparison between the experimental and calculated values using different models (Figure 7) shows that the Sips model produced the best fitting isotherm parameter values. The success of Sips isotherm model in the present system indicates that the surface heterogeneity of Fe(III)–AM-PGMACell was also contributing to phosphate adsorption. The applicability of the isotherm models for the present experimental data approximately follows the order: Sips > Langmuir > Freundlich. The adsorption capacity corresponding to all three models exhibited a significant decrement with increasing temperature, which is an indication of the exothermic nature of the process. The equilibrium constant b, relating to binding energy exhibited decrement suggesting the contribution of weaker binding sites at higher temperatures. As temperature increases, the stronger binding sites are primarily occupied and the binding strength decreases gradually with increasing degree of site occupation [25]. The value of q_{max} calculated from the Sips isotherm model at 20 °C was found to be 77.2 mg · g^{-1} for Fe(III)–AM-PGMACell, which was very much higher than the value 12.65 mg · g^{-1} for iron oxide tailings reported in the literature [26].

The essential characteristics of a Sips isotherm can be expressed in terms of a dimensionless constant separation factor R_s which is defined as:

$$R_s = \frac{1}{1 + b_s C_0^{1/n_s}}, \tag{7}$$

where b_s and $1/n_s$ are the Sips constants and C_0 is the initial concentration. The values of R_s were determined for different concentrations and temperatures and were in the range 0–1, which belongs to the type of favourable adsorption according to McKay et al. [27].

3.7. *Thermodynamic analysis of adsorption data*

The thermodynamic analysis was performed using the data from the plot represented in Figure 7. The apparent equilibrium constant (K_C) of the sorption is defined as:

$$K_C = \frac{C_{ad.eq}}{C_{eq}}, \tag{8}$$

where $C_{ad.eq}$ and C_{eq} are concentration of phosphate ions on the adsorbent and residual phosphate ion concentration at equilibrium, respectively. The values of ln K_C were determined and found to be 10.89, 9.35, 8.39 and 7.43 at 20, 30, 40 and 50 °C, respectively. The values of K_C were used to calculate thermodynamic parameters. The temperature dependence of adsorption process is associated with changes in thermodynamic parameters such as free energy (ΔG°), enthalpy

(ΔH°) and entropy (ΔS°) and was obtained using the following relationships:

$$\Delta G^\circ = -RT\ln K_C, \tag{9}$$

$$\ln K_C = \frac{\Delta S^\circ}{R} - \frac{\Delta H^\circ}{RT}, \tag{10}$$

where R is the ideal gas constant 8.314 ($J \cdot mol^{-1} \cdot K^{-1}$) and T is temperature (K). The values of ΔG° at temperatures 20, 30, 40 and 50 °C were found to be −26.54, −23.56, −21.85 and −19.96 $kJ \cdot mol^{-1}$, respectively. Negative values of ΔG° are indicative of the spontaneous nature of the adsorption process and confirm affinity of the adsorbent for the phosphate. The decrease in the negative ΔG° with temperature clearly shows that the adsorption is more favourable at low temperatures. Therefore, low temperatures favour the adsorption of phosphate ions onto Fe(III)–AM-PGMACell. Deliyanni et al. have reported the exothermic behaviour of phosphate adsorption on synthetic nanocrystalline akaganéite [28].

Plotting of ln K_C vs. $1/T$ (van't Hoff plot, not shown) gives a straight line with a slope and intercept equal to $\Delta H^\circ/RT$ and $\Delta S^\circ/R$, respectively. The negative value of ΔH° (−89.52 $kJ \cdot mol^{-1}$) indicates that phosphate adsorption is exothermic in nature, which is supported by the decrease in the adsorption onto Fe(III)–AM-PGMACell with a rise in temperature, as shown in Figure 7. High negative metal–ligand [Fe(III)–phosphate] heats are characteristics of metal ions coordinated with phosphate ligands, whereas coordination with carboxyl groups results in large positive enthalpy changes [29] The negative value of the entropy change, ΔS° (−216.05 $J \cdot mol^{-1} \cdot K^{-1}$) reflects the good affinity of phosphate ions towards the sorbent and the decreasing randomness at the solid–solution interface during the adsorption process. Isothermal data at four different temperatures were used to estimate the isosteric heat of adsorption process (ΔH_x) and is calculated using Clausius–Clapeyron equation [30]:

$$\frac{d(\ln C_e)}{dt} = -\frac{\Delta H_x}{RT^2}. \tag{11}$$

The plots of ln C_e vs. $1/T$ (not shown) for different amounts of phosphate adsorption were found to be linear. The values of ΔH_x were calculated from the slopes of the plots and were found to be −21.91, −22.36, −23.56, −24.51, −25.32, 26.23 and −28.10 $kJ \cdot mol^{-1}$ for the surface loading of 35.0, 37.0, 40.0, 42.0, 45.0, 47.0 and 50.0 $mg \cdot g^{-1}$, respectively, which are in the order of magnitude of that of physical adsorption [31]. The negative value of ΔH_x suggests the exothermic nature of the adsorption process. The magnitude of ΔH_x increases with the increase in concentration, suggesting higher sorption capacity at higher concentration. The isosteric heat of adsorption varies with the surface loading, indicating that the Fe(III)–AM-PGMACell used is an energetically heterogeneous surface. The variation in ΔH_x with surface loading is usually attributed to the presence of some lateral interactions between adsorbed molecules.

3.8. *Test with fertiliser industrial wastewaters*

The utility of adsorbent was demonstrated using real industrial wastewater. Industrial wastewater collected from a local fertiliser industry situated in Cochin city, India was characterised using standard methods [14] and the composition is Pb(II), 1.9 $mg \cdot L^{-1}$; Cd(II), 1.1 $mg \cdot L^{-1}$; Hg(II), 0.8 $mg \cdot L^{-1}$; Cl^-, 169.9 $mg \cdot L^{-1}$; NO_3^-, 79.1 $mg \cdot L^{-1}$; NO^{2-}, 15.3 $mg \cdot L^{-1}$; SO_4^{2-}, 134.3 $mg \cdot L^{-1}$; PO_4^{3-}, 11.6 $mg \cdot L^{-1}$; F^-, 0.98 $mg \cdot L^{-1}$; total NH_3, 414.9 $mg \cdot L^{-1}$; total hardness 89.7 $mg \cdot L^{-1}$; chemical oxygen demand, 238.7 $mg \cdot L^{-1}$; biological oxygen demand, 104.5 $mg \cdot L^{-1}$; dissolved oxygen, 3.3 $mg \cdot L^{-1}$; pH 5.0. The variations in phosphate removal efficiency with adsorbent dose are shown in Figure 8. From the figure it is evident that for the

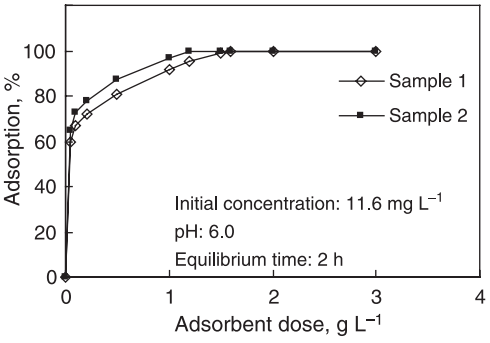

Figure 8. Effect of adsorbent dose on the adsorption of phosphate ions from industrial wastewater.

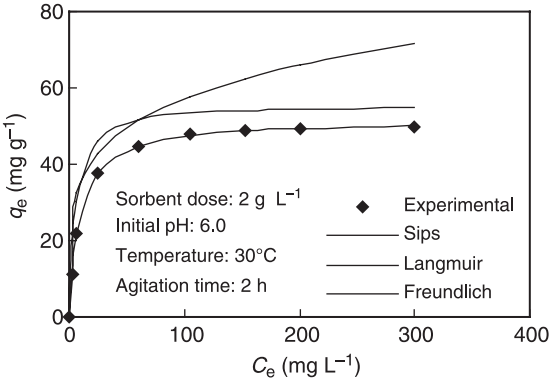

Figure 9. Comparison of experimental isotherm data and calculated isotherm data for the adsorption of phosphate on Dowex.

quantitative removal of phosphate ion from 1.0 L wastewater containing 25 mg · L^{-1} and several other ions (Sample 1); an adsorbent dosage of 1.6 g is sufficient for the complete removal of ∼100.0% of the total phosphate ion, whereas 2 g is required for the complete removal from the synthetic phosphate solution (Sample 2) having the same concentration (11.6 mg · L^{-1}) without any interfering ions. The reduction in phosphate adsorption from real industry wastewater might be ascribed to the competitive effect of concomitant anions and cations.

3.9. *Comparison with a commercial anion exchanger*

An adsorption isotherm study was conducted to determine the adsorption capacity of synthetic polymer based anion exchange resin. For this a commercial chloride form anion exchange resin Dowex, having a quaternary amine functionality and ion-exchange capacity of 4.2 meq · g^{-1}, was used. The experimental isotherm data obtained with 0.1 g of resin Dowex with different concentrations of phosphate ranging from 25 to 400 mg · L^{-1} at pH 6.0 and 30 °C are shown in Figure 9. The values of the Sips constant q_{max} and b were determined using non-linear regression analysis and were found to be 40.23 mg · g^{-1} and 0.325 L · mg^{-1} lower than that of Fe(III)–AM-PGMACell (70.11 mg · g^{-1} and 0.515 L · mg^{-1}). The results show that Fe(III)–AM-PGMACell is a better adsorbent for the removal of phosphate from aqueous solutions.

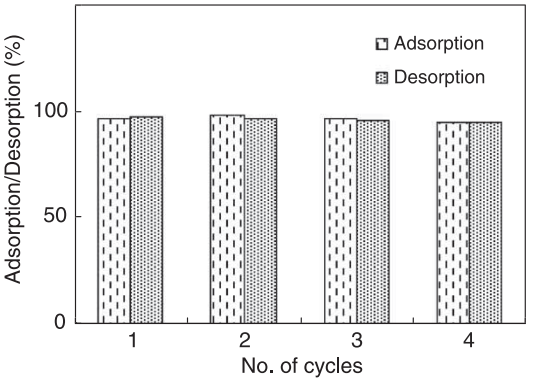

Figure 10. Adsorption–desorption plot for the removal of phosphate from aqueous solutions onto Fe(III)–AM-PGMACell.

3.10. *Cost factor*

The cost-effective and economical removal of phosphate from water and wastewater can be done by using low-cost and easily available adsorbents. The precursor used in the present study, commercial cellulose, was obtained at a cost $\$7.90 \cdot kg^{-1}$. After considering the expense of chemicals, electrical energy and manpower, the final developed adsorbent, Fe(III)–AM-PGMACell, cost $\sim\$220.00 \cdot kg^{-1}$. The cost of the commercially available anion exchanger Dowex (Aldrich, WI, USA) is $\$269.00 \cdot kg^{-1}$. The manufacturing cost of Fe(III)–AM-PGMACell is lower than the market cost of Dowex. The cost to remove 1.0 g phosphate ions from solution using Fe(III)–AM-PGMACell is ~1.7 times lower than the cost if using the commercial ion-exchange resins. Fe(III)–AM-PGMACell may also be used for the removal of arsenate, chromate and vanadate from aqueous solution, because the Cl^- ions in the Fe(III)–AM-PGMACell can exchange with toxic oxyanionic metals and is thus expected to bring down the cost.

3.11. *Evaluation of phosphate desorption*

From the cost and environmental points of view, a practical method of recycling the saturated adsorbent is necessary. Desorption of phosphate from spent adsorbent with 0.001, 0.005, 0.01 and 0.1 M NaCl resulted in 60.1, 71.2, 87.7 and 99.2% recovery of phosphate, respectively. A solution of 0.1 M NaCl was assumed to be the most suitable desorption agent. The high reversibility of phosphate adsorption on Fe(III)–AM-PGMACell indicates that the mechanism governing the adsorption process is ion exchange followed by the formation of outer sphere complexes with weak forces. The feasibility of an adsorption–desorption cyclic operation was also examined. The results are presented in Figure 10. In the four regeneration experiments, the adsorption capacity of Fe(III)–AM-PGMACell decreased gradually with the used cycle, but the adsorption capacity of regenerated adsorbent was always >95.0% that of the fresh Fe(III)–AM-PGMACell (Figure 10), which meant that the Fe(III)–AM-PGMACell possessed a good regenerability.

4. Conclusions

A new kind of adsorbent, cellulose-based anion exchanger [Fe(III)–AM-PGMACell] prepared by graft copolymerisation of cellulose with glycidyl methacrylate in the presence of MBA as a cross-linker using benzoyl peroxide initiator, followed by treatment with ethylenediamine and ferric

chloride in the presence of HCl, promises to be a prospective material for removing phosphate from aqueous solutions. FTIR, XRD and SEM were used to characterise the adsorbent. The optimum pH for phosphate adsorption was found to be in the range 5.0–7.0, which may be due to the monovalent species ($H_2PO_4^-$) in aqueous solution and the mechanism is supposed to be ion exchange. The adsorption process was rapid and equilibrium was attained in 120 min. Adsorption of phosphate followed two-step pseudo-first-order rate kinetics. The isotherm data were fitted with three adsorption isotherm models, Langmuir, Freundlich and Sips by non-linear regression. The experimental data correlated reasonably well with Sips adsorption isotherm and the isotherm parameters were calculated. The thermodynamic parameters revealed that the process was exothermic and spontaneous. Quantitative removal of 11.6 mg $\cdot$ L^{-1} phosphate ion in 1.0 L of industrial wastewater was achieved by 1.6 g of the adsorbent at pH 6.0 and 30 °C. Regeneration of the adsorbent could be achieved by 0.1 M NaCl solution for several cycles without any considerable reduction in its adsorption capacity. Based on the above results, the newly developed Fe(III)–AM-PGMACell can be effectively used as an alternative adsorbent for the removal and recovery of phosphate ions from water and wastewater.

Acknowledgements

The authors are thankful to the Head of the Department of Chemistry, University of Kerala, Thiruvananthapuram, India, for providing the laboratory facilities.

References

[1] J. Das, B.S. Patra, N. Baliarsingh, and K.M. Parida, *Adsorption of phosphate by layered double hydroxides in aqueous solutions*, Appl. Clay Sci. 32 (2006), pp. 252–260.
[2] D.G. Grubb, M.S. Guimaraes, and R. Valencia, *Phosphate immobilization using acidic type F fly ash*, J. Hazard. Mater. 76 (2000), pp. 217–236.
[3] C.P. Huang, *Adsorption of phosphate at the g Al_2O_3 electrolyte*, J. Colloid Interface Sci. 53 (1975), pp. 178–186.
[4] S.E. Bailey, T.J. Olin, R.M. Bricka, and D.D. Adrian, *A review of potentially low-cost sorbents for heavy metals*, Water Res. 33 (1999), pp. 2469–2479.
[5] N.I. Chubar, V.A. Kanibolotskyy, V.V. Strelko, G.G. Gallios, V.F. Samanidou, T.O. Shaposhnikova, V.G. Milgrandt, and I.Z. Zhuravlev, *Adsorption of phosphate ions on novel inorganic ion exchangers*, Colloid Surf. A 255 (2005), pp. 55–63.
[6] G.S. Chauhan, L. Guleria, and R. Sharma, *Synthesis, characterization and metal ion sorption studies of graft copolymers of cellulose with glycidyl methacrylate and some comonomers*, Cellulose 12 (2005), pp. 97–110.
[7] B. Sami and N.B. Mohamed, *Modified cellulose fibres for adsorption of dissolved organic solutes*, Cellulose 13 (2006), pp. 81–94.
[8] M.A. Tshabalala, K.G. Karthikeyan, and D. Wang, *Cationized milled pine bark as an absorbent for orthophosphate anions*, J. Appl. Polym. Sci. 93 (2004), pp. 1577–1583.
[9] R.X. Liu, J.L. Guo, and H.X. Tang, *Adsorption of fluoride, phosphate, and arsenate ions on a new type of ion exchange fiber*, J. Colloid Interf. Sci. 248 (2002), pp. 268–274.
[10] P.L. Xue, D. Yun, W. Bi, and S. Bi, *Adsorption behavior of phosphate on metal-ions-loaded collagen fiber*, Ind. Eng. Chem. Res. 45 (2006), pp. 3896–3901.
[11] J.A. Munoz, A. Gonzalo, and M. Valiente, *Kinetic and dynamic aspects of arsenic adsorption by Fe(III)-loaded sponge*, J. Soln. Chem. 37 (2008), pp. 553–565.
[12] X. Zhu and S.D. Alexandratos, *Polystyrene-supported amines: affinity for mercury(II) as a function of the pendant groups and the Hg(II) counterion*, Ind. Eng. Chem. Res. 44 (2005), pp. 8605–8610.
[13] J.A. Schwarz, C.T. Driscoll, and A.K. Bhanot, *The zero point charge of silica-alumina oxide suspension*, J. Colloid Interf. Sci. 97 (1984), pp. 55–61.
[14] American Public Health Association (APHA), *Standard Methods for the Examination of Water and Wastewater*, 18th ed., APHA, AWWA and WEF, Washington, DC, 1992.
[15] T.S. Anirudhan, B.F. Noelin, and D.M. Manohar, *Phosphate removal from wastewaters using a weak anion exchanger prepared from a lignocellulosic residue*, Environ. Sci. Technol. 40 (2006), pp. 2740–2745.
[16] D.D. Perrin and B. Dempsey, *Buffers for pH and Metal Ion Control*, Chapman & Hall, London, 1974, pp. 156–162.
[17] A.K. Golder, A.N. Samanta, and S. Ray, *Removal of phosphate from aqueous solutions using calcined metal hydroxides sludge waste generated from electrocoagulation*, Sep. Purif. Technol. 52 (2006), pp. 102–109.
[18] M. Yalvac and E. Can, *Phosphate removal from water by fly ash: factorial experimental design*, J. Hazard. Mater. 135 (2006), pp. 165–170.

[19] Y.Y. Qin, L. Qian, Y.G. Bao, and W. Yan, *Kinetics of adsorption of disperse dyes by polyepichlorohydrin-dimethylamine cationic polymer/bentonite*, Sep. Purif. Technol. 54 (2007), pp. 279–290.
[20] S.C. Biswas and D.K. Chattoraj, *Kinetics of adsorption of cationic surfactants at silica water interface*, Colloid Interface Sci. 205 (1998), pp. 12–20.
[21] W.J. Weber Jr and J.C. Morris, *Removal of biologically resistant pollutants from waste waters by adsorption*, in *Advances in Water Pollution Research. Proceedings of the 1st International Conference*, B.A. Southgate, ed., Pergamon Press, New York, 1962, pp. 231–266.
[22] I. Langmuir, *The adsorption of gases on plane surfaces of glass, mica and platinum*, J. Am. Chem. Soc. 40 (1918), pp. 1361–1403.
[23] H.M.F. Freundlich, *Over the adsorption in solution*, J. Phys. Chem. 57 (1906), pp. 385–470.
[24] R. Sips, *On the structure of a catalyst surface*, J. Chem. Phys. 16 (1948), pp. 490–495.
[25] I. Ruzic, *Trace metal complexation at heterogeneous binding sites in aquatic systems*, Mar. Chem. 53 (1996), pp. 1–15.
[26] Z. Le, X. Li, and J. Liu, *Adsorptive removal of phosphate from aqueous solutions using iron oxide tailings*, Water Res. 38 (2004), pp. 1318–1326.
[27] G. Mckay, H.S. Blair, and J.R. Garden, *Adsorption of dyes on chitin equilibrium study*, J. Appl. Polymer Sci. 27 (1982), pp. 3043–3057.
[28] E.A. Deliyanni, E.N. Peleka, and N.K. Lazaridis, *Comparative study of phosphates removal from aqueous solutions by nanocrystalline akaganeite and hybrid surfactant-akaganeite*, Sep. Purif. Technol. 52 (2007), pp. 478–486.
[29] J. Romero-González, J.R. Peralta-Videa, E. Rodríguez, S.L. Ramirez, and J.L. Gardea-Torresdey, *Determination of thermodynamic parameters of Cr(VI) adsorption from aqueous solutions onto* Agave lechuguilla *biomass*, J. Chem. Thermodyn. 37 (2005), pp. 343–347.
[30] D.M. Young and A.D. Crowell, *Physical Adsorption of Gases*, Butterworth, London, 1962.
[31] T.S. Anirudhan and P.G. Radhakrishnan, *Kinetics, thermodynamics and surface heterogeneity assessment of uranium(VI) adsorption onto cation exchange resin derived from a lignocellulosic residue*, Appl. Surf. Sci. 255 (2009), pp. 4983–4991.